PASSIVE SUPPRESSION OF AEROELASTIC INSTABILITIES OF IN-FLOW WINGS BY TARGETED ENERGY TRANSFERS TO LIGHTWEIGHT ESSENTIALLY NONLINEAR ATTACHMENTS

Young S. Lee[1], **Alexander F. Vakakis**[2], **Lawrence A. Bergman**[1], **D. Michael McFarland**[1], **and Gaëtan Kerschen**[3]

[1]Department of Aerospace Engineering
University of Illinois at Urbana-Champaign, Urbana, IL 61801, USA
e-mail: yslee4@uiuc.edu, lbergman@uiuc.edu, dmmcf@uiuc.edu

[2]Mechanics Division, School of Applied Mathematical and Physical Sciences
National Technical University of Athens, Athens, Greece
e-mail: vakakis@central.ntua.gr

[3]Aerospace and Mechanical Engineering Department (LTAS)
Université de Liège, Liège, Belgium
e-mail: g.kerschen@ulg.ac.be

Keywords: Limit cycle oscillation, targeted energy transfer, nonlinear energy sink.

Abstract. Theoretical and experimental suppression of aeroelastic instabilities by means of broadband passive targeted energy transfers has been recently studied. A single-degree-of-freedom (SDOF) nonlinear energy sink (NES) was coupled to a 2-DOF rigid wing modeled in the low-speed, subsonic regime with quasi-steady aerodynamic theory. The nonlinear attachment was designed and optimized to suppress the critical nonlinear modal energy exchanges between the flow and the (pitch and heave) wing modes, thus suppressing the (transient) triggering mechanism of aeroelastic instability. We performed bifurcation analysis to find regions of robust passive aeroelastic suppression in parameter space. Then, we employed multi-degree-of-freedom nonlinear energy sinks (MDOF NESs) to improve robustness of the aeroelastic instability suppression. Bifurcation analysis by a numerical continuation technique demonstrated that controlling the occurrence of a limit point cycle (LPC or saddle-node) bifurcation point above a Hopf bifurcation point is crucial to enhancing suppression robustness. MDOF NESs not only can enhance robustness of suppression against even strong gust-like disturbances, but they require lower NES mass compared to SDOF NES designs. The validity of the theoretical findings was proven by a series of wind tunnel experiments.

1 INTRODUCTION

Classical linear theory predicts that a flexible wing will exhibit divergent response at flow speeds above a critical flutter speed, implying that catastrophic failure will occur when this critical speed is exceeded. Fortunately, real structures are often sufficiently nonlinear, displaying hardening stiffness for example, that their response at supercritical speeds takes the form of a steady limit cycle oscillation (LCO) rather than diverging. Even when they do not cause damage, such oscillations are extremely undesirable because they limit the operating envelope of high-performance aircraft such as the F-16 and F/A-18 [1, 2].

Many authors have studied the causes of LCOs. The common factor in all aircraft systems exhibiting limit cycle behavior is aeroelastic nonlinearities. These nonlinearities can exist in the flow field, the structure, or both. Dowell et al. [3] provides an excellent summary of recent

studies done in the fields of aerodynamics and structural dynamics to understand nonlinear aeroelasticity.

Regarding methods for controlling or suppressing LCOs, several control laws such as linear theory, partial feedback linearization, and adaptive control have been utilized to stabilize an inherently unstable aeroelastic system with a single trailing edge control surface [4] or with leading and trailing edge control surfaces [5]. These studies have shown that active control can be used to raise the threshold velocity above which LCOs occur. While active control has been shown to be effective in suppressing LCOs, these methods require significant use of control resources. Active methods also require sensors capable of constantly providing accurate measurements of the system state for feedback into the controller.

On the other hand, targeted energy transfer (alternatively, nonlinear energy pumping) refers to the irreversible transfer of vibration energy from the main structure of a dynamic system to an attachment with essentially nonlinear (nonlinearizable) stiffness and linear damping. Vakakis and Gendelman [6] and Vakakis et al. [7] showed that when the essentially nonlinear oscillator resonates with a mode of the main system, energy is transferred (pumped) from the main system to the nonlinear attachment irreversibly. The attachment thus acts as a nonlinear energy sink (NES), which is a completely passive device with no state measurement or energy input required.

The NES has been developed and studied at the University of Illinois at Urbana-Champaign [6, 7, 8, 9, 10]. Unlike a linear dynamic absorber, which is effective in narrow frequency bands, the NES works against broadband disturbances. In addition, while the linear absorber is a steady-state device, the NES provides transient protection as well.

Lee et al. [11] showed the applicability of nonlinear energy pumping to suppress the LCO of a van der Pol oscillator, which is analogous to a nonlinear aeroelastic problem. The LCO suppression mechanism was found to be a series of captures into, and escapes from, resonances, from superharmonic to subharmonic order. This successful demonstration of NES applicability to suppress a self-excited instability was, in particular, the catalyst for the present work, which provides both analytical and experimental demonstrations of suppressing aeroelastic instability with a nonlinear energy sink.

2 ANALYTICAL STUDY

2.1 System descriptions

We consider the 2-DOF in-flow rigid wing coupled to a single-DOF ungrounded NES (Fig. 1). The main motivation for considering this configuration lies in the LCO triggering mechanism[12] in the wing with no NES attached; that is, an initial excitation of the heave mode of the wing acts as the triggering mechanism for the development of LCOs with the wing oscillating predominantly in its pitch mode. Because both the initial excitation (trigger) of the heave mode and the eventual development of the LCO are transient phenomena, a successful strategy for aeroelastic instability suppression should address directly the transient problem before the full LCO has developed.

Assuming small motions and quasi-steady aerodynamics, one can derive the nondimensional

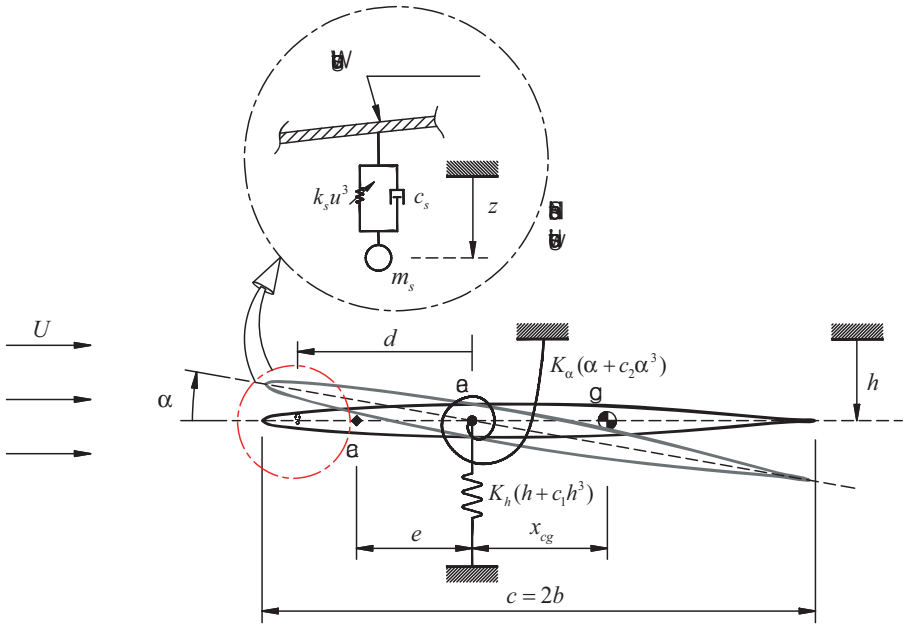

Figure 1: 2-DOF rigid wing model coupled with an SDOF NES (ac, ea, and cg stand for the aerodynamic center, elastic axis, and center of gravity, respectively).

equations of motion of the wing-NES assembly as

$$\begin{aligned} y'' + x_\alpha \alpha'' + \Omega^2 y + \xi_y y^3 + \mu C_{L,\alpha} \Theta \left(y' + \Theta\alpha\right) & \\ + \varepsilon\lambda \left(y' - \delta\alpha' - v'\right) + C\left(y - \delta\alpha - v\right)^3 &= 0 \\ r_\alpha^2 \alpha'' + x_\alpha y'' + r_\alpha^2 \alpha + \xi_\alpha \alpha^3 - \gamma\mu C_{L,\alpha} \Theta \left(y' + \Theta\alpha\right) & \\ + \delta\varepsilon\lambda \left(\delta\alpha' + v' - y'\right) + \delta C\left(\delta\alpha + v - y\right)^3 &= 0 \\ \varepsilon v'' + \varepsilon\lambda \left(v' + \delta\alpha' - y'\right) + C\left(v + \delta\alpha - y\right)^3 &= 0 \end{aligned} \tag{1}$$

where y, α, and v are the heave, pitch, and NES displacements, respectively; x_α, the static mass unbalance of the wing (positive aft of the ea); Ω, the ratio of the uncoupled linear natural frequencies for the heave and pitch modes; ξ_y and ξ_α, the coefficients for the cubic nonlinear terms; μ, the density ratio; Θ, the reduced velocity; $C_{L,\alpha}$, the slope of the lift curve; r_α, the radius of gyration of the wing; γ, the location of the ac measured from the ea (positive ahead of the ea); ε, λ, and C, the NES mass, damping, and coefficient of the essential nonlinearity, respectively; and δ, the offset attachment of the NES (positive ahead of the ea). We adopted the system parameters for this study,

$$x_\alpha = 0.2,\ r_\alpha = 0.5,\ \gamma = 0.4,\ \Omega = 0.5,\ \mu = (10\pi)^{-1},\ C_{L,\alpha} = 2\pi,\ \xi_y = \xi_\alpha = 1$$

giving a flutter speed $\Theta_F = 0.87$.

2.2 Suppression mechanisms

Three distinct mechanisms for suppressing aeroelastic instability by means of targeted energy transfers are identified; that is, recurring suppressed burst-outs, partial suppression, and complete suppression of instability. A synoptic presentation of the three basic LCO suppression mechanisms identified in the numerical simulations is provided in the following, focusing on their main dynamical features.

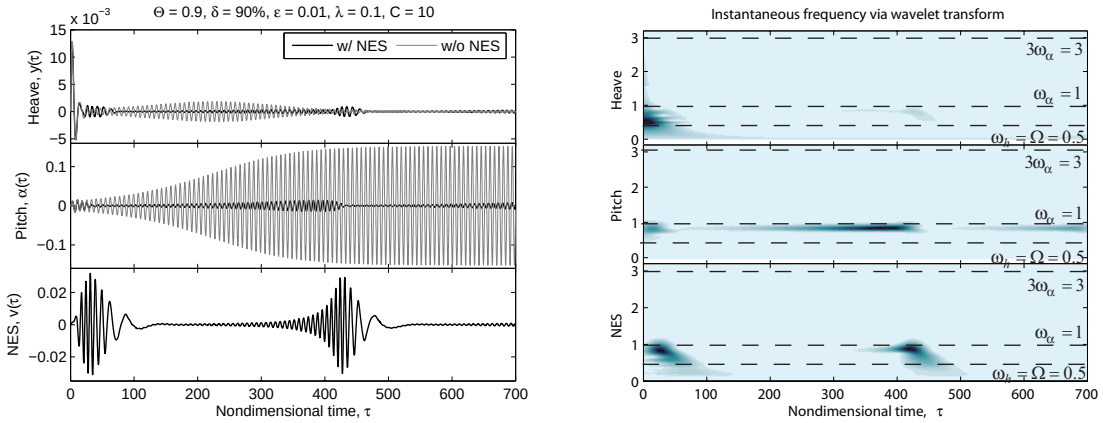

(a) Time responses (b) Wavelet transforms

Figure 2: The first suppression mechanism when $\Theta = 0.9$, $\delta = 90\%$, $\varepsilon = 1\%$, $\lambda = 0.1$, and $C = 10$. All initial conditions were zero except $y'(0) = 0.01$.

The first suppression mechanism (Fig. 2) This mechanism is characterized by *a recurrent series of suppressed burst-outs of the heave and pitch modes of the wing, followed by eventual complete suppression of the aeroelastic instabilities*. In the initial phase of transient burst-outs, a series of developing instabilities of predominantly the heave mode is effectively suppressed by proper transient 'activation' of the NES, which tunes itself to the fast frequency of the developing aeroelastic instability; as a result, the NES engages in 1:1 transient resonance capture (TRC) with the heave mode, passively absorbing broadband energy from the wing, thus eliminating the burst-out. In a later phase of the dynamics, the energy fed by the flow does not appear to directly excite the heave and pitch modes of the wing but, instead, to get transferred directly to the NES until the wing is entirely at rest and complete LCO suppression is achieved. At the initial stage of the recurrent burst-outs, at time instants when the pitching LCO is nearly eliminated, most of the energy induced by the flow to the wing is absorbed directly by the NES with only a small amount being transferred to the heave mode, so that both the NES and the heave mode reach their maximum amplitude modulations. This is followed by suppression of the burst-out, a process that is repeated until at a later stage complete suppression of the aeroelastic instability is reached. The beating-like (quasi-periodic) modal interactions observed during the recurrent burst-outs turn out to be associated with Neimark-Sacker bifurcations [13] of a periodic solution and to be critical for determining domains of robust suppression.

The second suppression mechanism (Fig. 3) *Intermediate suppression of LCOs* is the typical behavior in this case, and is commonly observed when there occurs partial LCO suppression. The initial action of the NES is the same as in the first suppression mechanism. Targeted energy transfer to the NES then follows under conditions of 1:1 TRC, followed by conditions of 1:1 permanent resonance capture (PRC) where both heave and pitch modes attain constant (but nonzero) steady-state amplitudes. We note that the heave mode response can grow larger than in the corresponding system with no NES attached (exhibiting an LCO), while suppressing the pitch mode. We also note that, in contrast to the first suppression mechanism, the action of the NES is nonrecurring in this case, as it acts at the early phase of the motion stabilizing the wing and suppressing the LCO.

The third suppression mechanism (Fig. 4) In this mechanism energy transfers from the wing

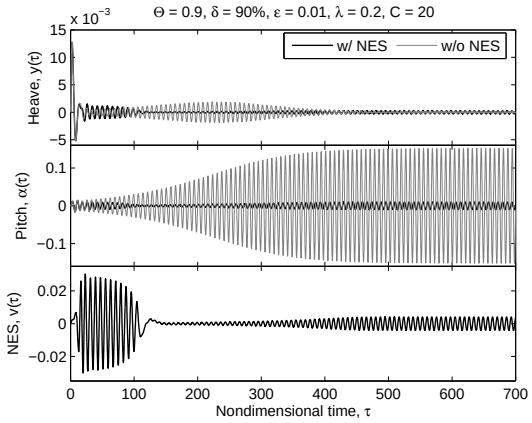

(a) Time responses

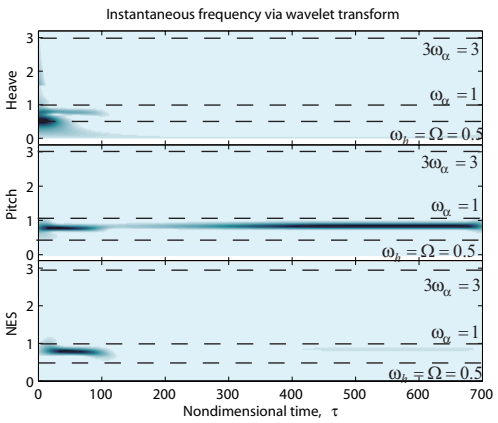

(b) Wavelet transforms

Figure 3: The second suppression mechanism when $\Theta = 0.9$, $\delta = 90\%$, $\varepsilon = 1\%$, $\lambda = 0.2$, and $C = 20$. All initial conditions were zero except $y'(0) = 0.01$.

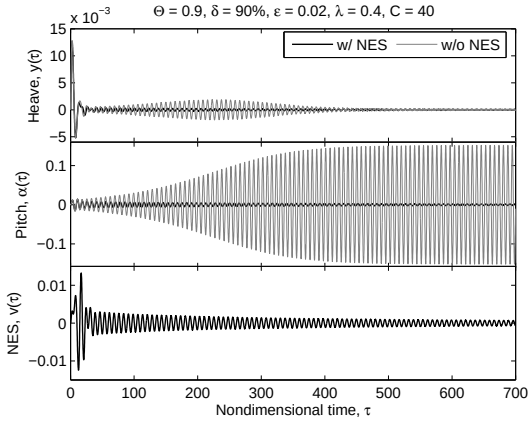

(a) Time responses

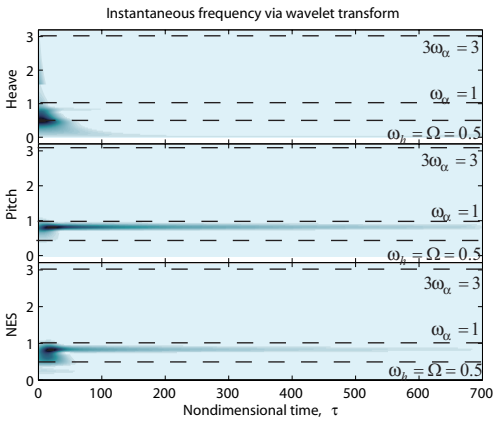

(b) Wavelet transforms

Figure 4: The third suppression mechanism when $\Theta = 0.9$, $\delta = 90\%$, $\varepsilon = 1\%$, $\lambda = 0.4$, and $C = 40$. All initial conditions were zero except $y'(0) = 0.01$.

to the NES are caused by nonlinear modal interactions during 1:1 RCs. Both heave and pitch modes as well as the NES exhibit exponentially decaying responses resulting in *complete elimination of LCOs*.

In order to analytically prove that the LCO suppression is due to resonance captures, one can utilize the complexification-averaging technique [14]. Based on the wavelet transform (WT) results in Figs. 2–4, we assume the multifrequency decomposition for the heave, pitch and NES transient responses,

$$y(\tau) = y_1(\tau) + y_2(\tau),\ \alpha(\tau) = \alpha_1(\tau) + \alpha_2(\tau),\ v(\tau) = v_1(\tau) + v_2(\tau) \tag{2}$$

where the components with subscripts 1, 2 correspond to slow modulations of the fast frequency components, $e^{j\Omega\tau}$, $e^{j\tau}$, respectively. Specifically, the two fast frequencies are the two natural frequencies of the heave and pitch modes in the uncoupled linearized system; we designate these

components as LF (lower-frequency) and MF (middle-frequency) components, respectively, for notational convenience and also for consistency with the notation used in Lee et al. [12].

Introducing the new complex variables[14]

$$\begin{aligned} \psi_1 &= y_1' + j\Omega y_1,\ \psi_3 = y_2' + j y_2;\ \psi_2 = \alpha_1' + j\Omega\alpha_1,\ \psi_4 = \alpha_2' + j\alpha_2; \\ \psi_5 &= v_1' + j\Omega v_1,\ \psi_6 = v_2' + j v_2; \end{aligned} \tag{3}$$

we express the original variable for the heave mode in the form

$$\begin{aligned} y &= \frac{1}{2j\Omega}(\psi_1 - \psi_1^*) + \frac{1}{2j}(\psi_3 - \psi_3^*) \\ y' &= \frac{1}{2}(\psi_1 + \psi_1^*) + \frac{1}{2}(\psi_3 + \psi_3^*) \\ y'' &= \psi_1' + \psi_3' - \frac{j\Omega}{2}(\psi_1 + \psi_1^*) - \frac{j}{2}(\psi_3 + \psi_3^*) \end{aligned} \tag{4}$$

Similar expressions hold for the variables corresponding to the pitch mode and the NES.

Substitute the previous expressions into the equations of motion (1), expressing the complex variables in polar form, $\psi_1(\tau) = \varphi_1(\tau)e^{j\Omega\tau}$, $\psi_3(\tau) = \varphi_3(\tau)e^{j\tau}$; $\psi_2(\tau) = \varphi_2(\tau)e^{j\Omega\tau}$, $\psi_4(\tau) = \varphi_4(\tau)e^{j\tau}$; $\psi_5(\tau) = \varphi_5(\tau)e^{j\Omega\tau}$, $\psi_6(\tau) = \varphi_6(\tau)e^{j\tau}$, where $\varphi_i(\tau)$ is the slowly-varying complex-valued amplitude modulation of the respective fast-varying component $e^{j\Omega\tau}$ or $e^{j\tau}$. Applying two-frequency averaging over the two fast components, $e^{j\Omega\tau}$ and $e^{j\tau}$, we obtain a set of six complex-valued modulation equations governing the slow-flow dynamics,

$$\varphi' = \mathbf{F}(\varphi) \tag{5}$$

where $\varphi \in \mathbb{C}^6$; the details of $\mathbf{F}$ are not included here.

Introducing the final polar-form expressions, $\varphi_i(\tau) = a_i(\tau)e^{jb_i(\tau)}$ where $a_i(\tau),\ b_i(\tau) \in \mathbb{R},\ i = 1,\ 2, \ldots,\ 6$, we express the set of six (complex-valued) slow flow modulation equations (5) in terms of a set of twelve (real-valued) modulation equations governing the slow evolutions of the amplitudes and phases,

$$\mathbf{a}' = \mathbf{f}(\mathbf{a}, \varphi),\ \varphi' = \mathbf{g}(\mathbf{a}, \varphi) \tag{6}$$

where $\mathbf{a} \in \mathbb{R}_+^6$ and $\varphi \in S^6$. The slowly-varying amplitudes $a_1,\ a_3$ ($a_2,\ a_4$; $a_5,\ a_6$) are respectively LF and MF components of the heave (pitch; NES) mode. The independent phase angle vector φ possesses the components $\varphi_{ij} = b_i - b_j$. Note that all independent phase interactions occur between same frequency components (LF-LF or MF-MF).

Resonance captures and escapes can be illustrated by the phase interactions in Fig. 5. An interesting observation is that the resonance captures between the heave and pitch modes occur ahead of those between the heave mode and NES, or those between the pitch mode and NES. This implies that in the first suppression mechanism there occur nonlinear modal energy exchanges between the heave and pitch modes (i.e., the triggering mechanism [12] is activated) before TET to the NES (with the ensuing instability suppression) occurs. This early occurrence of RCs between the heave and pitch modes makes the repetition of suppression and burst-out in the first suppression mechanism possible.

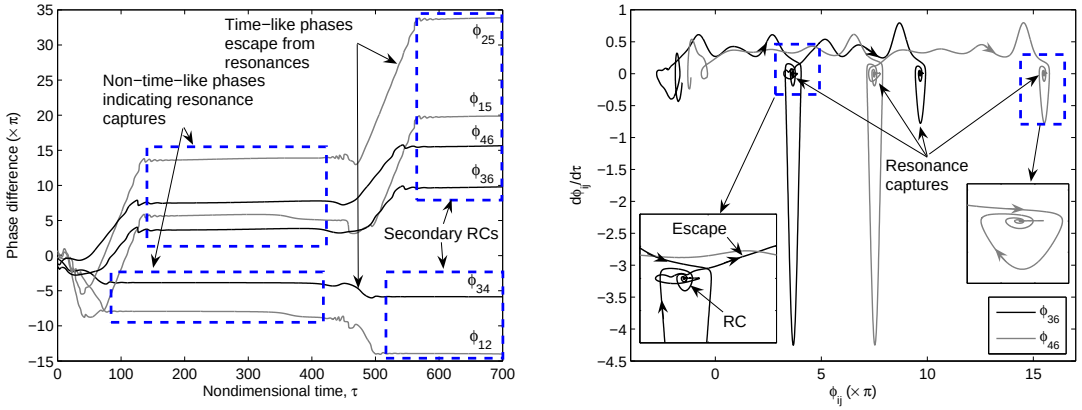

(a) (b)

Figure 5: Analytical suppression mechanism via two-frequency averaging technique for the first mechanism shown in Fig. 2.

3 EXPERIMENTAL STUDY

The nonlinear aeroelastic test apparatus (NATA) at Texas A&M University was developed to experimentally test linear and nonlinear aeroelastic behavior. The low-speed wind tunnel with a 3ft width $\times$ 2ft height $(0.91 \times 0.51\text{m})$ test section is a closed-circuit type with capacity of air speeds up to 45m/s. The device consists of a rigid NACA 0015 wing section capable of movement with two DOF, pitch and heave (Fig. 6 (a)).

Experiments using the NATA are conducted at very low speeds and at very low reduced frequency. The wing section spans the entire wind tunnel, so the flow can be considered two-dimensional. For this flow environment, lift and drag can be modeled with quasi-steady aerodynamics. This type of aerodynamic model has provided very good agreement with NATA experimental results in the past, which can be referred to for the NATA parameters [4, 5].

For the first proof-of-concept experiments with an NES in an aerodynamic application, the design goals were similar to what would be desired of flight hardware, tempered by the realities of the laboratory environment and the scale of the test program. It was expected to design a light-weight, passive, self-contained attachment that would significantly improve the dynamic response of the NATA under typical operating conditions. On the basis of previous studies [15], values of the stiffness and damping were selected, then refined through a series of numerical simulations, carried out using MATLAB.

A typical experimental bifurcation diagram with the standard NES[15] is presented in Fig. 6 (b). The dashed lines with triangles represent the results with this typical NES parameters. The flutter speed is significantly increased from 9m/s to 11m/s (22% improvement). Moreover, transitions appear sequentially from the third to second suppression mechanism.

Figure 6 (c) depicts the first suppression mechanism observed when the flow speed $U = 11$m/s, and the NES of a lighter mass, weaker stiffness and higher damping was applied. As in the theory, both the aeroelastic modes and the NES exhibit a nonlinear beating phenomenon; i.e., recurring burst-out and suppression of aeroelastic instability. The frequency ratio of the two aeroelastic modes exhibits 1:1 relation around 2–3 Hz by counting the number of waves per a

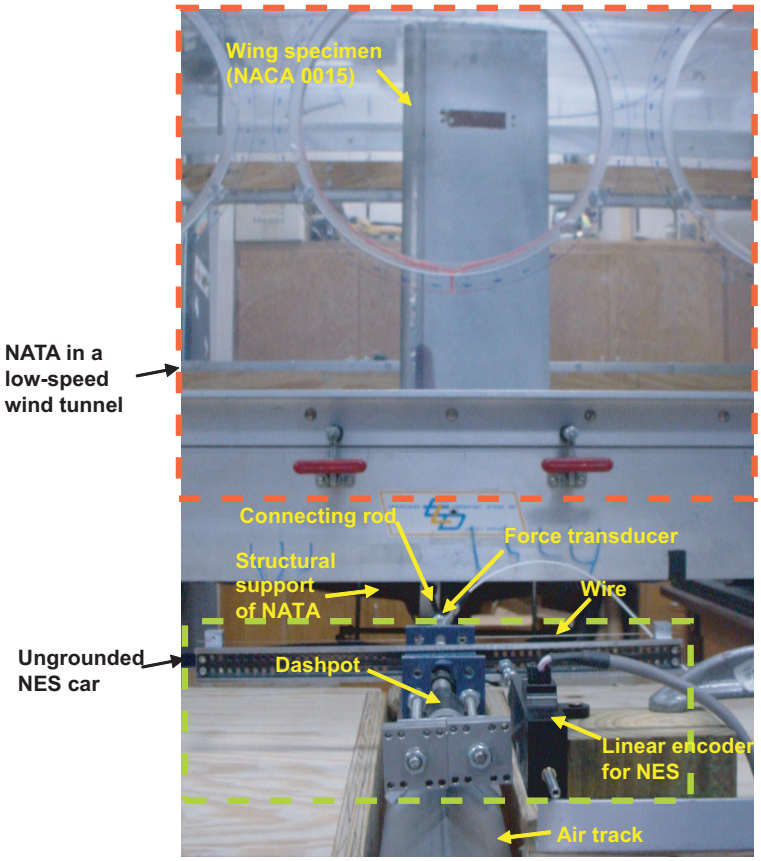

(a) Experimental setup for the NATA coupled to NES

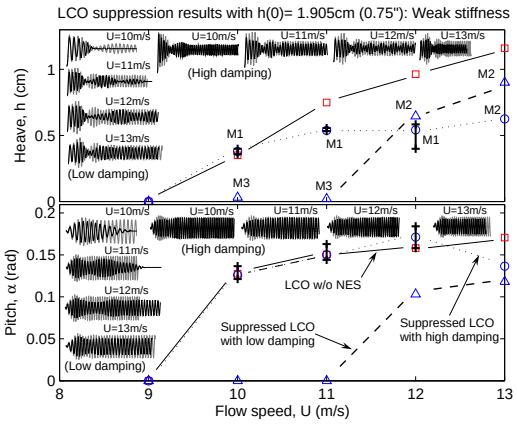

(b) Typical experimental results

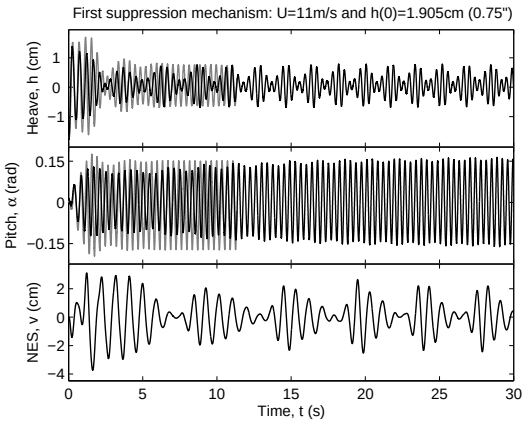

(c) Typical aeroelastic responses of the wing exhibiting recurring suppressed burst-outs

Figure 6: Data taken for the NES with $m_s = 1.2$kg, weak essentially-nonlinear stiffness, and all zero initial conditions except for $h(0) = 1.905$cm ($= 0.75$in.). The solid lines with square symbol indicate the LCO responses of the NATA when the NES is not applied; the dashed lines with triangles (the dotted lines with circles) represent for the suppressed LCOs when low (high) damping is used. $M1$, $M2$, and $M3$ denote the first, second, and third suppression mechanisms of LCOs, respectively. Amplitude modulations are denoted by a line between two '+' symbols.

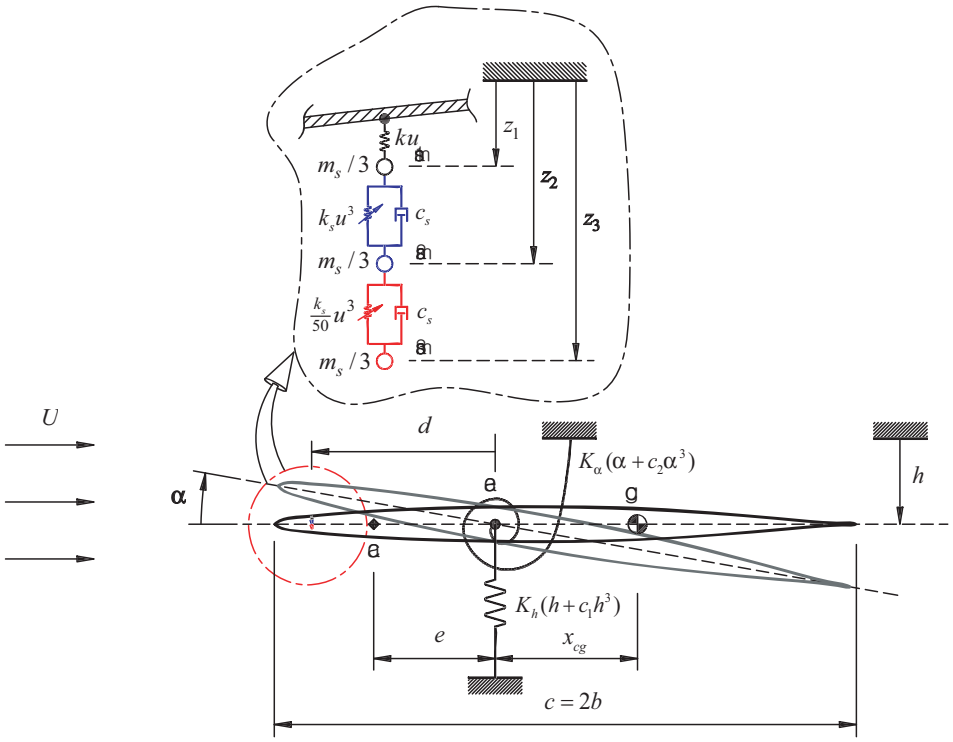

Figure 7: Application of an MDOF NES in series coupling for the 2-DOF rigid wing.

second. On the other hand, the frequency ratio between the NES and heave (or pitch) mode becomes a 1:2 (or 1:3) subharmonic.

This observation can suggest that this first suppression mechanism predominantly consists of recurring (or transient) subharmonic resonance captures between the NES and aeroelastic modes, while the two aeroelastic modes are continually in 1:1 internal resonance exchanging the respective modal energy.

4 ENHANCING ROBUSTNESS OF SUPPRESSION WITH A MDOF NES

In order to improve robustness of instability suppression compared to an SDOF NES, we consider an MDOF NES configuration, shown in Fig. 7. This kind of MDOF NESs in series coupling was studied in Tsakirtzis et al. [16], basically showing that application of the MDOF NESs can induce even richer dynamics on the frequency-energy plot (FEP) [8]. This means, in turn, that there exists higher possibility for a system to possess more 'baits' to seize the dynamics caused by any disturbances onto a branch in the FEP, making it stick to (or, at least, very close to) the branch until a significant amount of energy is dissipated by a damper in the process of resonance captures.

The MDOF NES is composed of the three equal masses, which in total make the same mass ratio as the SDOF NES. The first mass of the MDOF NES is coupled to a wing only through a linear stiffness, and its main role is a 'bridge' for efficient energy transfers from the wing to the other nonlinear attachments. The second and third ones coupled through essentially nonlinear stiffnesses. The best performance is achieved when the order of the essential nonlinearity between the second and third masses is much smaller than than between the first and second masses; the former is set 50 times less than the latter.

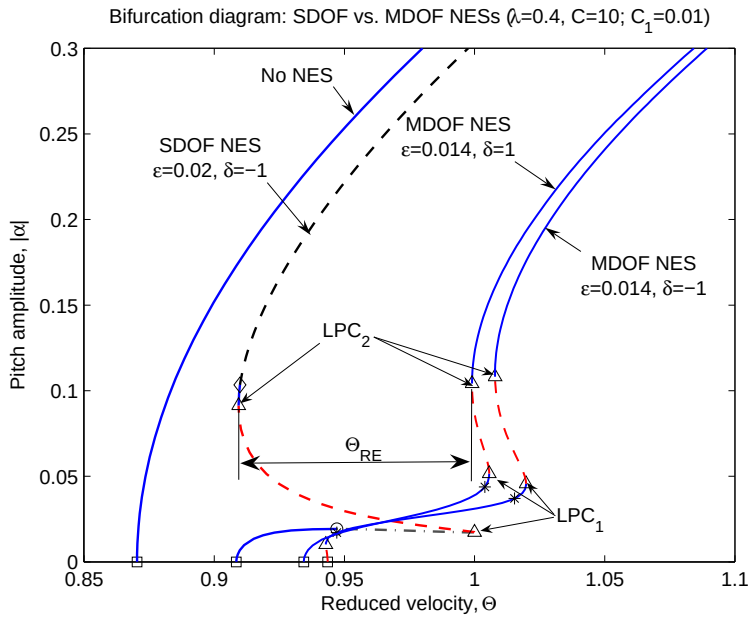

Figure 8: Comparison of bifurcation diagrams: SDOF versus MDOF NESs ($\lambda = 0.4$, $C = 10$, $C_1 = 0.01$). The SDOF NES is considered with the mass ratio $\varepsilon = 0.02$ and the offset $\delta = -1$. The MDOF NES is equipped with $\varepsilon = 0.014$, $\delta = \pm 1$. Dashed lines indicate unstable LCO branches. Squares (circles, triangles, diamond, asterisks) indicate Hopf (Neimark-Sacker, limit point of cycles or saddle-node, branch point of cycles, neutral-saddle) bifurcation points. Θ_{RE} denotes the amount of the enhanced reduced speed for robustness.

The nondimensional equations of motion can be written

$$\begin{aligned}
&y'' + x_\alpha \alpha'' + \Omega^2 y + \xi_y y^3 + \mu C_{L,\alpha} \Theta \left(y' + \Theta \alpha\right) + C_1 \left(y - \delta\alpha - v_1\right) = 0 \\
&r_\alpha^2 \alpha'' + x_\alpha y'' + r_\alpha^2 \alpha + \xi_\alpha \alpha^3 - \gamma \mu C_{L,\alpha} \Theta \left(y' + \Theta \alpha\right) + \delta C_1 \left(\delta\alpha + v_1 - y\right) = 0 \\
&\tfrac{1}{3}\varepsilon v_1'' + \varepsilon\lambda \left(v_1' - v_2'\right) + C_1 \left(v_1 + \delta\alpha - y\right) + C \left(v_1 - v_2\right)^3 = 0 \\
&\tfrac{1}{3}\varepsilon v_2'' + \varepsilon\lambda \left(v_2' - v_1'\right) + \varepsilon\lambda \left(v_2' - v_3'\right) + C \left(v_2 - v_1\right)^3 + \tfrac{1}{50} C \left(v_2 - v_3\right)^3 = 0 \\
&\tfrac{1}{3}\varepsilon v_3'' + \varepsilon\lambda \left(v_3' - v_2'\right) + \tfrac{1}{50} C \left(v_3 - v_2\right)^3 = 0
\end{aligned} \tag{7}$$

Then, numerical bifurcation analysis by means of MatCont [17] is performed to examine changes in LCO branches. A typical result is depicted in Fig. 8. For the purpose of comparison, the LCO branches without an NES and with an SDOF NES are superimposed. The coefficients of the damping and essential nonlinearity are the same for both NES configurations; the mass ratios (ε) for the SDOF and MDOF NESs are 0.02 and 0.014, respectively. The offset attachments (δ) for both are selected as ± 1.

Robustness enhancement at a relatively high reduced velocity is demonstrated in Fig. 9, where the mass ratio of 2% (1.4%) is considered for the SDOF (MDOF) NES. The aeroelastic system controlled by the MDOF NES exhibits robustness against the impulsive disturbance to the heave mode at the steady state (Fig. 9 (b)), whereas there exists a transition from lower-amplitude unstable quasi-periodic LCO branch to higher-amplitude stable stable LCO branch for the control only with the SDOF NES (Fig. 9 (a)).

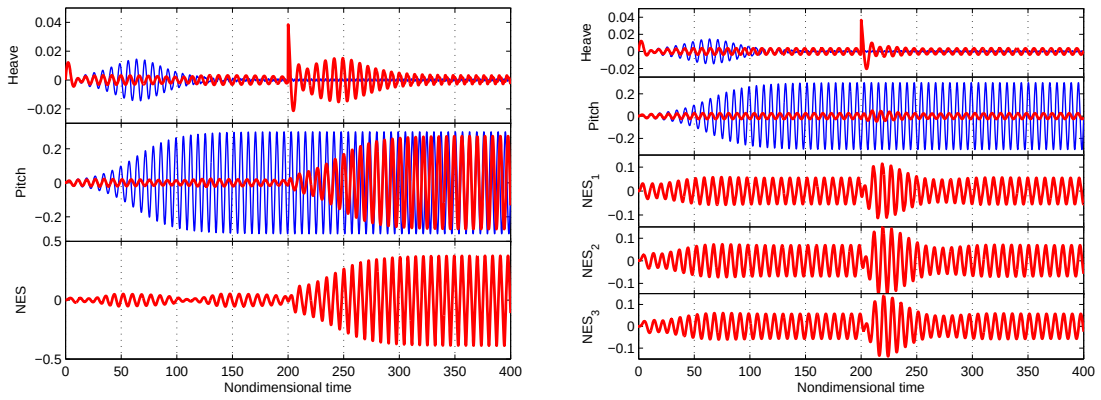

(a) (b)

Figure 9: Demonstration of enhancing robust suppression of instability under the impulsive disturbance of $20 \times y'(0)$ at $\tau = 200$ when $\Theta = 0.98$, $\delta = -1$, $\lambda = 0.4$, $C = 10$, $C_1 = 0.01$ (a) with an SDOF NES ($\varepsilon = 0.02$), and (b) with an MDOF NES ($\varepsilon = 0.014$). The thick lines indicate the controlled responses.

4.1 Targeted Energy Transfers (TETs)

We now investigate the TET mechanisms in the case of MDOF NESs. As a first step, wavelet transforms (WTs) are performed to examine the instantaneous frequency behaviors (i.e., transient resonant interactions between the aeroelastic and NES modes), as are summarize in the following.

The WT involves a windowing technique with variable-sized regions so that it performs a multi-resolution analysis, in contrast to the (fast) Fourier transform (FFT) which assumes signal stationarity. Small time intervals are considered for high-frequency components whereas the size of the interval is increased for lower-frequency components, thereby giving better time and frequency resolutions than the FFT. The Matlab® codes used for the WT computations in this work were developed at the Université de Liège (Liège, Belgium) by Dr. V. Lenaerts in collaboration with Dr. P. Argoul from the Ecole Nationale des Ponts et Chaussées (Paris, France). The Morlet wavelet, $\psi_M(\tau) = e^{-\tau^2/2} e^{j\omega_0 \tau}$, which is a Gaussian-windowed complex sinusoid of frequency ω_0, is considered as a mother wavelet in this study. The frequency ω_0 for the Morlet WT is a user-specified parameter which allows one to tune the frequency and time resolutions of the results. The plots represent the amplitude of the WT as a function of frequency (vertical axis) and time (horizontal axis). Heavily shaded areas correspond to regions where the amplitude of the WT is high, whereas lightly shaded regions correspond to low amplitudes. Such plots enable one to deduce the temporal evolution of the dominant frequency components of the signals analyzed. Comparing the instantaneous frequency contents of the aeroelastic and NES modes provides an additional (direct) way to verify the occurrence of resonance captures, or frequency locking in the transient dynamics.

The instantaneous kinetic and potential energies, which are stored in the masses and springs,

respectively, can be written:

$$\begin{aligned}\bar{T}(\tau) &= \tfrac{1}{2}y'(\tau)^2 + x_\alpha y'(\tau)\alpha'(\tau) + \tfrac{1}{2}\alpha'(\tau)^2 + \tfrac{1}{3}\varepsilon\left[v_1'(\tau)^2 + v_2'(\tau)^2 + v_3'(\tau)^2\right] \\ \bar{V}(\tau) &= \tfrac{1}{2}\Omega^2 y(\tau)^2 + \tfrac{1}{2}r_\alpha^2\alpha(\tau)^2 + \tfrac{1}{4}\xi_y y(\tau)^4 + \tfrac{1}{4}\xi_\alpha\alpha(\tau)^4 \\ &\quad + \tfrac{1}{4}C\left[v_1(\tau) - v_2(\tau)\right]^4 + \tfrac{1}{200}C\left[v_2(\tau) - v_3(\tau)\right]^4 + \tfrac{1}{2}C_1\left[y(\tau) - \delta\alpha(\tau) - v_1(\tau)\right]^2\end{aligned} \tag{8}$$

so that the total energy can be computed from

$$E^{Total}(\tau) = \bar{T}(\tau) + \bar{V}(\tau) \tag{9}$$

The energy input from the flow, which is a sum of the initial energy provided by the initial conditions and the nonconservative work done by the flow, can be expressed

$$E^{Input}(\tau) = E^{Total}(0) + W_{nc}^{y}(\tau) + W_{nc}^{\alpha}(\tau) \tag{10}$$

where

$$\begin{aligned}W_{nc}^{y}(\tau) &= \mu C_{L,\alpha}\Theta\int_0^\tau \left\{y'(s) + \Theta\alpha(s)\right\}y'(s)ds \\ W_{nc}^{\alpha}(\tau) &= -\gamma\mu C_{L,\alpha}\Theta\int_0^\tau \left\{y'(s) + \Theta\alpha(s)\right\}\alpha'(s)ds\end{aligned}$$

The total energy dissipation by the MDOF NES can be written

$$E_d^{NES}(\tau) = E_d^{NES1}(\tau) + E_d^{NES2}(\tau) \tag{11}$$

where

$$E_d^{NES1}(\tau) = \varepsilon\lambda\int_0^\tau \left[v_1'(s) - v_2'(s)\right]^2 ds,\; E_d^{NES2}(\tau) = \varepsilon\lambda\int_0^\tau \left[v_2'(s) - v_3'(s)\right]^2 ds \tag{12}$$

As a result, the following instantaneous energy balance should hold:

$$E^{Total}(\tau) = E^{Input}(\tau) - E_d^{NES}(\tau) \tag{13}$$

We set the flow speed as $\Theta = 0.92$, for which a complete elimination of aeroelastic instability can be realized (see Fig. 8). For all zero initial conditions except for $y\prime(0) = 0.1$, one obtains the responses shown in Fig. 10 (a). Initial transients exhibits beating-like interactions between the aeroelastic and NES modes. One can see, from Fig. 10 (c), that a significant amount of energy is extracted to the MDOF NES masses in the first two big interactions (i.e., $\tau \in [0, 100]$; E^y, E^α, E^u, E^v and E^w respectively denote the energies contained the heave and pitch modes, the first, second, and the third of the MDOF NES). Moreover, a balance between the energy input and the energy dissipation by the NES is reached in this period. It should be desirable that more energy dissipation occurs in the second damper (i.e., $E_d^{NES1} < E_d^{NES2}$), which demonstrates more energy is transferred to the third mass than the second mass. Also, WTs in Fig. 10 (b) proves that there exist strong nonlinear modal interactions involving transient resonance captures [12] in this period.

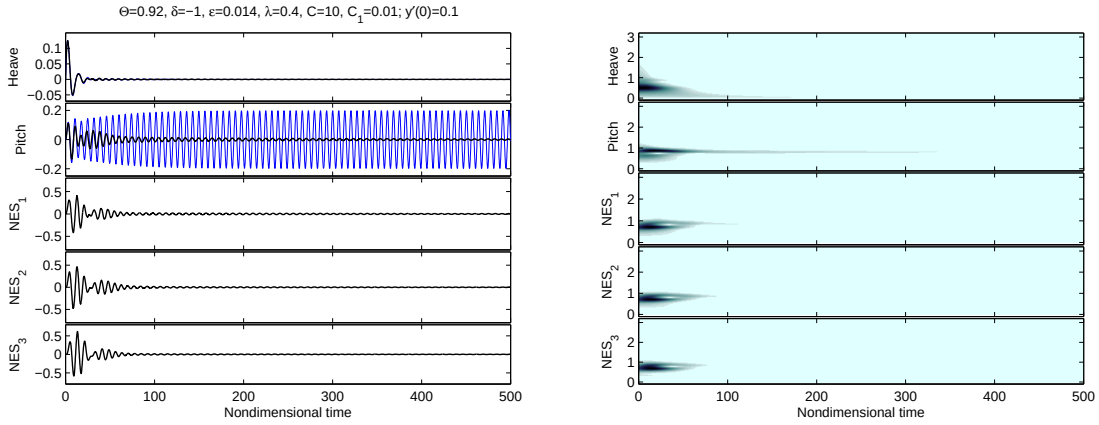

(a) (b)

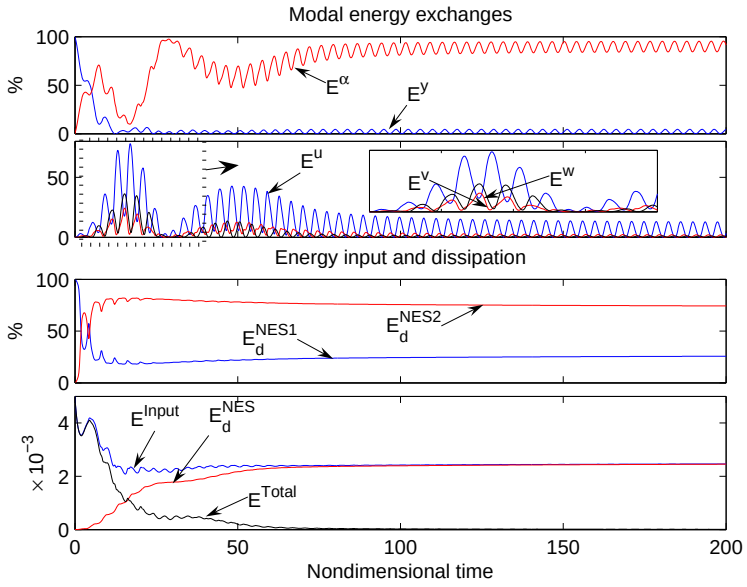

(c)

Figure 10: Wing responses when the MDOF NES is applied ($\Theta = 0.92$, $\varepsilon = 0.014$, $\lambda = 0.4$, $C = 10$, $C_1 = 0.01$, $\delta = -1$, $y\prime(0) = 0.1$): (a) Time series (thin lines for uncontrolled responses); (b) wavelet transforms; (c) energy exchanges between the aeroelastic and NES modes.

Another interesting observation, which is not included in this paper, is that, for a smaller $y\prime(0)$, it takes longer time to reach a steady state (i.e., a balance between the input energy and energy dissipation). Also, the smaller disturbances yield energy transfer mechanism which make the second mass possess the more energy than the third one. Different from the case with a strong $y\prime(0)$, more energy dissipation occurs in the first damper (i.e., $E_d^{NES1} > E_d^{NES2}$). This observation again proves that more efficient nonlinear energy pumping can be realized for sufficiently large input energy (see, for example, Vakakis and Gendelman [6]). The MDOF NESs with a positive offset tend to exhibit less number of initial transient interactions.

5 CONCLUSIONS

Suppression of aeroelastic instability (or LCO) in a 2-DOF rigid wing by means of passive targeted energy transfers (TETs) was investigated. Three distinct mechanisms for LCO sup-

pression were identified both in theory and experiments: recurrent burst-outs and suppression, partial suppression and complete suppression. It was found that the passive TETs are activated by transient resonant interactions between the NES and the aeroelastic modes.

In order to improve robustness of aeroelastic instability suppression in a rigid wing with structural nonlinearities, we considered a MDOF NES configuration. From the bifurcation analysis of the dynamics of the integrated wing-NES system by means of a numerical continuation technique, we showed that the control of the occurrence of the lower LPC bifurcation point above a Hopf bifurcation point is crucial to enhancing robustness. Moreover, we demonstrated that the proposed MDOF NES design (composed of multiple masses coupled in series by means of essentially nonlinear springs and viscous dampers) not only greatly enhances the robustness of LCO suppression against even strong impulsive disturbances, but also achieves comparable or better suppression performance for smaller total masses compared to SDOF NESs under identical disturbances. Nonlinear modal interactions between the wing and the attached MDOF NES were studied by means of WTs, as well as the resulting modal energy exchanges.

The results reported in this work, which should be viewed in conjunction with earlier theoretical and experimental results[18, 19], indicate that appropriately designed lightweight passive nonlinear absorbers with essential stiffness nonlinearities can suppress LCO instabilities effectively and robustly.

ACKNOWLEDGMENTS

This work was supported by the US Air Force Office of Scientific Research through Grant Number FA9550–04–1–0073. GK was supported by a grant from the Belgian National Science Foundation, which is gratefully acknowledged.

REFERENCES

[1] C. M. Denegri, Jr. Limit cycle oscillation flight test results of a fighter with external stores. *Journal of Aircraft*, 37(5):761–769, 2000.

[2] R. W. Bunton and C. M. Denegri, Jr. Limit cycle oscillation characteristics of a fighter aircraft. *Journal of Aircraft*, 37(5):916–918, 2000.

[3] E. A. Dowell, J. Edwards, and T. W. Strganac. Nonlinear aeroelasticity. *Journal of Aircraft*, 40(5):857–874, 2003.

[4] J. Ko, A. J. Kurdila, and T. W. Strganac. Nonlinear control of a prototypical wing section with torsional nonlinearity. *Journal of Guidance, Control, and Dynamics*, 20:1181–1189, 1997.

[5] G. Platanitis and T. W. Strganac. Control of a nonlinear wing section using leading- and trailing-edge surfaces. *Journal of Guidance, Control, and Dynamics*, 27(1):52–58, 2004.

[6] A. F. Vakakis and O. Gendelman. Energy pumping in nonlinear mechanical oscillators: Part II—Resonance capture. *ASME Journal of Applied Mechanics*, 68:42–48, January 2001.

[7] Alexander F. Vakakis, D. Michael McFarland, Lawrence A. Bergman, Leonid I. Manevitch, and Oleg Gendelman. Isolated resonance captures and resonance capture

cascades leading to single- or multi-mode passive energy pumping in damped coupled oscillators. *ASME Journal of Vibration and Acoustics*, 126(2):235–244, April 2004.

[8] Young S. Lee, Gaetan Kerschen, Alexander F. Vakakis, Panagiotis Panagopoulos, Lawrence A. Bergman, and D. Michael McFarland. Complicated dynamics of a linear oscillator with a light, essentially nonlinear attachment. *Physica D: Nonlinear Phenomena*, 204(1–2):41–69, May 2005.

[9] Gaetan Kerschen, Young S. Lee, Alexander F. Vakakis, D. Michael McFarland, and Lawrence A. Bergman. Irreversible passive energy transfer in coupled oscillators with essential nonlinearity. *SIAM Journal on Applied Mathematics*, 66:648–679, 2006.

[10] D. Michael McFarland, Lawrence A. Bergman, and Alexander F. Vakakis. Experimental study of nonlinear energy pumping occurring at a single fast frequency. *International Journal of Nonlinear Mechanics*, 40(6):891–899, July 2005.

[11] Young S. Lee, Alexander F. Vakakis, Lawrence A. Bergman, and D. Michael McFarland. Suppression of limit cycle oscillations in the van der Pol oscillator by means of passive nonlinear energy sinks (NESs). *Structural Control and Health Monitoring*, 13(1):41–75, 2006.

[12] Young S. Lee, Alexander F. Vakakis, Lawrence A. Bergman, D. Michael McFarland, and Gaetan Kerschen. Triggering mechanisms of limit cycle oscillations due to aeroelastic instability. *Journal of Fluids and Structures*, 21(5–7):485–529, 2005.

[13] Y. Kuznetsov. *Elements of Applied Bifurcation Theory*. Springer-Verlag, New York, 1995.

[14] L. I. Manevitch. The description of localized normal modes in a chain of nonlinear coupled oscillators using complex variables. *Nonlinear Dynamics*, 25:95–109, 2001.

[15] D. Michael McFarland, Gaetan Kerschen, Jeffrey J. Kowtko, Lawrence A. Bergman, and Alexander F. Vakakis. Experimental investigation of targeted energy transfers in strongly and nonlinearly coupled oscillators. *Journal of the Acoustical Society of America*, 118(2): 791–799, August 2005.

[16] S. Tsakirtzis, P.N. Panagopoulos, G. Kerschen, O. Gendelman, A.F. Vakakis, and L.A. Bergman. Complex dynamics and targeted energy transfers in linear oscillators coupled to multi-degree-of-freedom essentially nonlinear attachments. *Nonlinear Dynamics*, 48(3): 285–318, May 2007.

[17] A. Dhooge, W. Govaerts, and Y.A. Kuznetsov. Matcont: A matlab package for numerical bifurcation analysis of odes. *ACM Transactions on Mathematical Software*, 29(2):141–164, 2003.

[18] Young S. Lee, Alexander F. Vakakis, Lawrence A. Bergman, D. Michael McFarland, and Gaëtan Kerschen. Suppression of aeroelastic instability by means of broadband passive targeted energy transfers, Part I: Theory. *AIAA Journal*, 45(3):693–711, 2007.

[19] Young S. Lee, Gaëtan Kerschen, D. Michael McFarland, W. Joel Hill, Chetan Nichkawde, Thomas W. Strganac, Lawrence A. Bergman, and Alexander F. Vakakis. Suppression of aeroelastic instability by means of broadband passive targeted energy transfers, Part II: Experiments. *AIAA Journal*, in review.